

Record High Cationic Dye Separation Performance for Water Sanitation Using a Neutral Coordination Framework

Zheng Wang[†], Cheng-Yi Zhu[†], Heng-Shun Zhao, Shao-Yun Yin, Su-Juan Wang, Jian-Hua Zhang, Ji-Jun Jiang, Mei Pan*, and Cheng-Yong Su

Lehn Institute of Functional materials, MOE Laboratory of Bioinorganic and Synthetic Chemistry, School of Chemistry, Sun Yat-Sen University, Guangzhou 510275, China.

1. Crystal structure of LIFM-WZ-4.....	2
2. IR, TGA and PXRD.....	6
3. Gases sorption isotherms (CO ₂ , CO, N ₂ , CH ₄ , C ₂ H ₆ , C ₂ H ₄ , C ₃ H ₆ and C ₃ H ₈).....	8
4. Calculation of adsorption isosteric heats.....	11
5. IAST selectivity	14
6. Organic dyes with different sizes and charges.....	21
7. Dye adsorption test results.....	22
8. Kinetic and thermodynamic feature research	28
9. References	33

1. Crystal structure of LIFM-WZ-4

Table S1. Crystal data and structure refinement for LIFM-WZ-4

Identification code	LIFM-WZ-4
Empirical formula	C ₄₈ H ₂₈ CoN ₂₀
Formula weight	943. 83
Temperature	150. 00(10)
Wavelength	1.54178 Å
Crystal system	Monoclinic
Space group	P2 ₁ /n
a, Å	12. 9310(11)
b, Å	13. 4843(10)
c, Å	15. 6502(11)
α, °	90
β, °	101. 310(8)
γ, °	90
V, Å ³	2675. 9(4)
Z	2
Calculated density	1. 171
Crystal size, mm	0. 19×0. 18×0. 17
Absorption coefficient	2. 929
F(000)	966. 0
Theta range for data collection	8. 128 to 127. 37
Limiting indices	-10≤h≤11, -13≤ k≤15, -22≤l≤24
Reflections collected	4321
Independent reflections	4321 [R(int) = 0.0652]
Completeness to theta = 65.99	98.2%
Refinement method	Full-matrix least-squares on F ²
Data/restraints/parameters	4321/1/313
Quality-of-fit indicator	1.024
Final R indices [I>2σ(I)]	R ₁ = 0. 0935, wR ₂ = 0. 1947
R indices (all data)	R ₁ = 0. 1358, wR ₂ = 0. 2079
Largest diff. peak and hole	0. 51/-0. 31 e.Å ⁻³

Table S2. Selected bond distances (Å) for LIFM-WZ-4

Co1-	N5¹	1.885(6)	C3	C4	1.439(9)
Co1-	N5 ²	1.885(6)	C4	C5	1.377(10)
Co1-	N2	1.964(5)	C5	C6	1.380(9)
Co1-	N2 ³	1.964(5)	C5	C11	1.501(9)
Co1-	N1 ³	1.977(5)	C6	C7	1.443(10)
Co1-	N1	1.977(5)	C7	C8	1.319(10)
N1-	C1	1.371(9)	C8	C9	1.427(10)
N1-	C4	1.372(8)	C9	C10	1.385(9)
N2-	C6	1.366(8)	C10	C13	1.365(9)
N2-	C9	1.381(9)	C10	C18	1.510(11)
N3-	C17	1.320(9)	C11	C16	1.342(11)
N3-	N4	1.361(9)	C11	C12	1.364(9)
N4	N5	1.296(9)	C12	C13	1.380(9)
N5	N6	1.325(6)	C13	C14	1.363(10)
N5	Co1 ⁴	1.885(6)	C14	C15	1.336(9)
N6	C17	1.298(9)	C14	C17	1.460(9)
N7	C2 ⁴	1.263(12)	C15	C16	1.394(10)
N7	N8	1.348(13)	C18	C23	1.366(11)
N8	N9	1.320(14)	C18	C19	1.397(12)
N9	N10	1.349(11)	C19	C20	1.403(13)
N10	C24	1.351(11)	C20	C21	1.349(12)
C1	C10 ³	1.365(9)	C21	C22	1.366(12)
C1	C2	1.428(9)	C21	C24	1.472(12)
C2	C3	1.310(10)	C22	C23	1.403(12)

Symmetry transformations used to generate equivalent atoms:

¹1/2+X,3/2-Y,1/2+Z; ²1/2-X,-1/2+Y,1/2-Z; ³-X,1-Y,1-Z; ⁴1/2-X,1/2+Y,1/2-Z**Table S3.** Selected bond angles (deg) for LIFM-WZ-4

N5¹	Co1	N5²	180.0(3)	C4	C5	C11	118.6(6)
N5¹	Co1	N2	91.2(2)	C6	C5	C11	118.9(7)
N5²	Co1	N2	88.8(2)	N2	C6	C5	125.9(7)
N5¹	Co1	N2 ³	88.8(2)	N2	C6	C7	110.4(6)
N5²	Co1	N2 ³	91.2(2)	C5	C6	C7	123.7(6)
N2	Co1	N2 ³	180.00(16)	C8	C7	C6	106.9(7)
N5¹	Co1	N1 ³	88.4(2)	C7	C8	C9	107.9(8)
N5²	Co1	N1 ³	91.6(2)	N2	C9	C10	125.5(6)
N2	Co1	N1 ³	90.9(2)	N2	C9	C8	110.0(6)
N2³	Co1	N1 ³	89.1(2)	C10	C9	C8	124.4(7)
N5¹	Co1	N1	91.6(2)	C1 ³	C10	C9	124.9(7)
N5²	Co1	N1	88.4(2)	C1 ³	C10	C18	117.9(6)
N2	Co1	N1	89.1(2)	C9	C10	C18	117.2(6)

N2³	Co1	N1	90.9(2)	C16	C11	C12	115.8(7)
N1³	Co1	N1	180.0	C16	C11	C5	124.4(7)
C1	N1	C4	105.4(5)	C12	C11	C5	119.8(7)
C1	N1	Co1	127.1(4)	C11	C12	C13	121.8(8)
C4	N1	Co1	127.4(5)	C14	C13	C12	121.4(7)
C6	N2	C9	104.8(6)	C15	C14	C13	117.4(7)
C6	N2	Co1	128.5(5)	C15	C14	C17	123.5(7)
C9	N2	Co1	126.4(4)	C13	C14	C17	119.1(6)
C17	N3	N4	104.9(7)	C14	C15	C16	120.7(8)
N5	N4	N3	109.5(6)	C11	C16	C15	123.1(8)
N4	N5	N6	106.8(6)	N6	C17	C14	109.4(6)
N4	N5	Co1 ⁴	124.2(4)	N6	C17	C14	126.1(7)
N6	N5	Co1 ⁴	128.6(5)	N3	C17	C14	124.1(7)
C17	N6	N5	108.9(6)	C23	C18	C19	116.9(9)
C24	N7	N8	106.8(10)	C23	C18	C10	121.2(8)
N9	N8	N7	109.2(10)	C19	C18	C10	121.9(8)
N8	N9	N10	107.1(10)	C18	C19	C20	120.8(10)
C24	N10	N9	105.4(9)	C21	C20	C19	120.1(10)
C10³	C1	N1	125.1(6)	C22	C21	C20	121.0(9)
C10³	C1	C2	125.2(7)	C22	C21	C24	121.2(10)
N1	C1	C2	109.6(6)	C20	C21	C24	117.8(10)
C3	C2	C1	108.1(7)	C21	C22	C23	118.5(9)
C2	C3	C4	107.4(6)	C18	C23	C22	122.7(9)
N1	C4	C5	126.6(6)	N7	C24	N10	111.5(9)
N1	C4	C3	109.5(6)	N7	C24	C21	126.1(11)
C5	C4	C3	123.9(6)	N10	C24	C21	122.4(11)
C4	C5	C6	122.2(6)				

¹-1/2+X,3/2-Y,1/2+Z; ²1/2-X,-1/2+Y,1/2-Z; ³-X,1-Y,1-Z; ⁴1/2-X,1/2+Y,1/2-Z

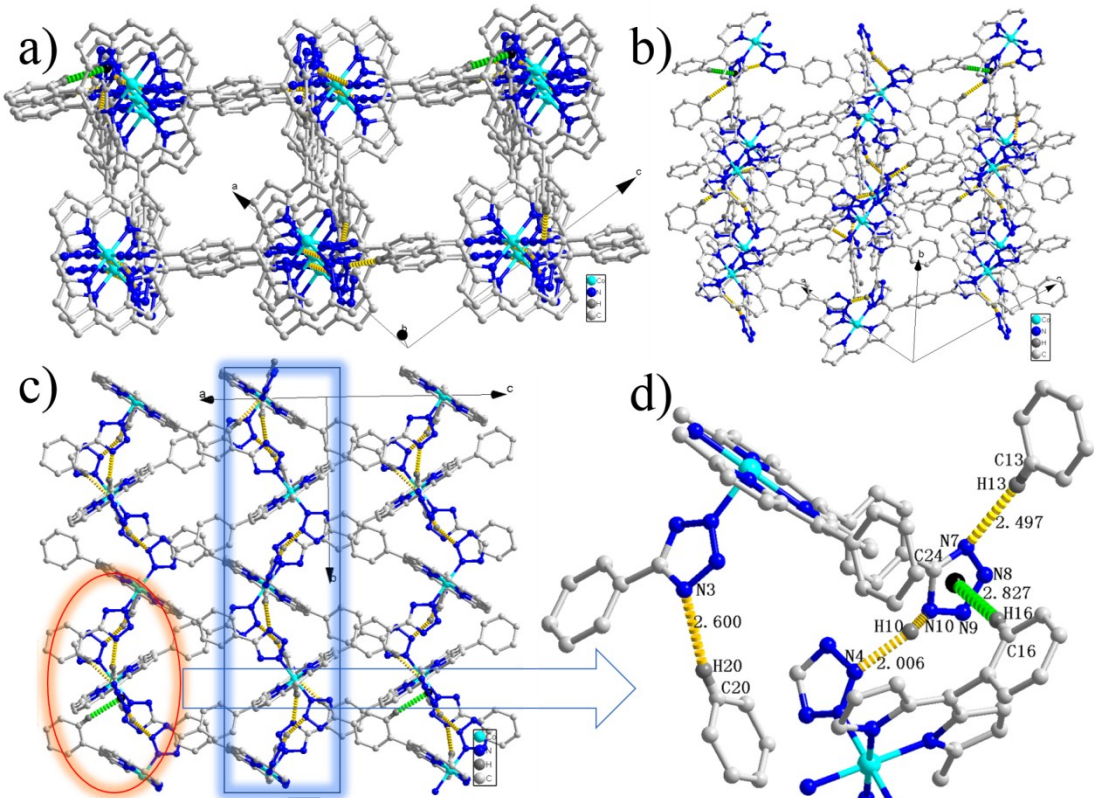


Figure S1. Crystal structure of LIFM-WZ-4. a, b and c) 3D nets formed via C–H...N, N–H...N and C–H... π stacking interactions; d) Enlargement moiety of figure c) to show more clearly the weak interactions: intermolecular N–H...N (2.006 Å for N₁₀-H₁₀...N₄), C–H...N (2.497 Å and 2.600 Å for C₁₃-H₁₃...N₇ and C₂₀-H₂₀...N₃) interactions (yellow line) and C–H... π (2.827 Å for C₁₆-H₁₆...Cg₁, Cg₁=N₇, N₈, N₉, N₁₀ and C₂₄) interactions (green line).

2. IR, TGA and PXRD

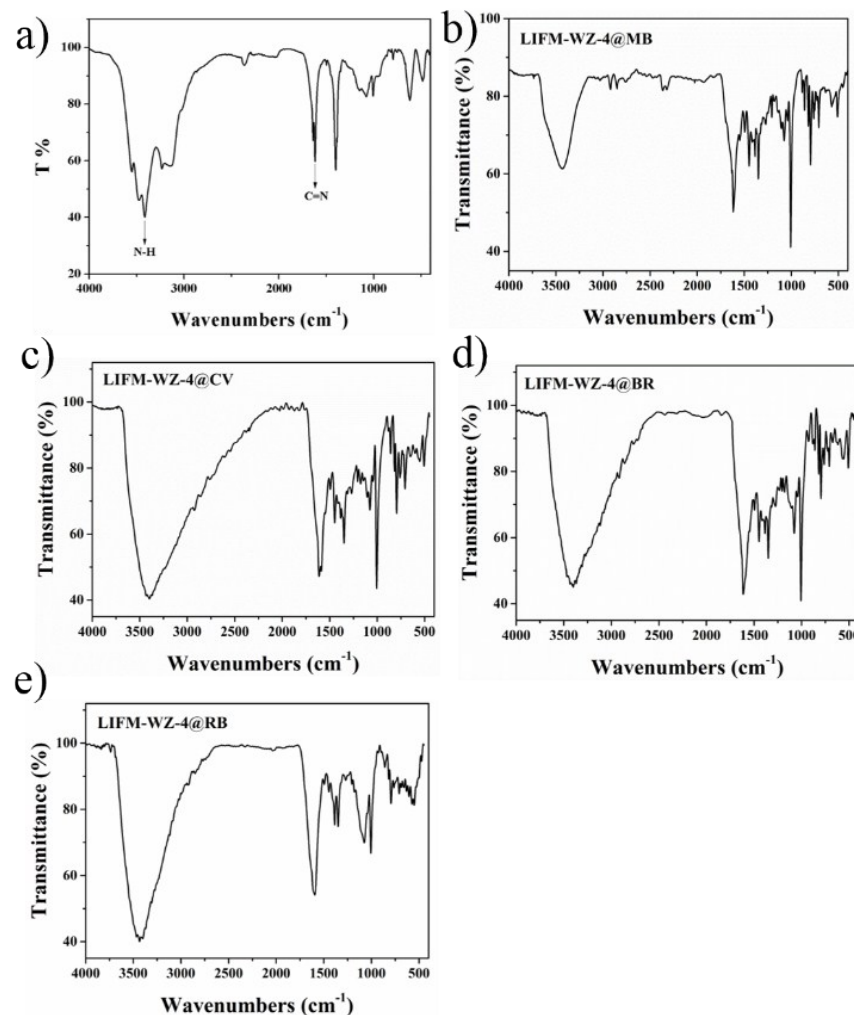


Figure S2. The Infrared spectra. a-e) LIFM-WZ-4, LIFM-WZ-4@MB, LIFM-WZ-4@CV, LIFM-WZ-4@BR, LIFM-WZ-4@RB, respectively.

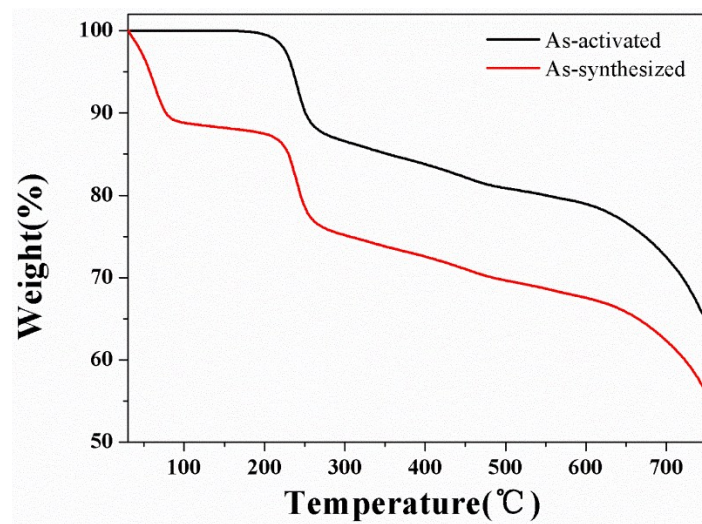


Figure S3. The TGA curve for LIFM-WZ-4

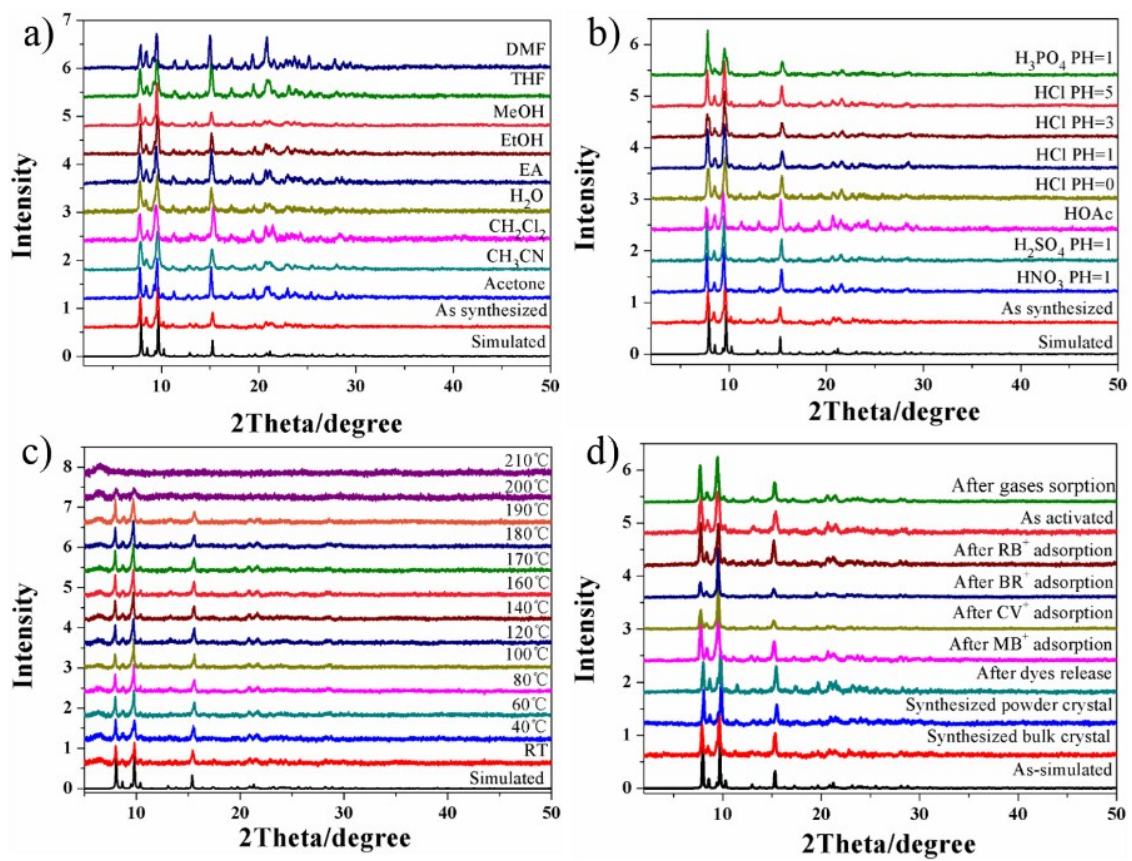


Figure S4. PXRD patterns of LIFM-WZ-4. a) Samples after soaking in aqueous solutions of different solvents, and b) samples after soaking in aqueous solutions of different pH values and acids for 72 h. c) Variable temperature PXRD from RT to 210 °C, and d) PXRD for samples after activation and gas sorption, and after dyes (MB^+ , CV^+ , BR^+ and RB^+) adsorption and release tests.

3. Gases sorption isotherms (CO_2 , CO , N_2 , CH_4 , C_2H_6 , C_2H_4 , C_3H_6 and C_3H_8)

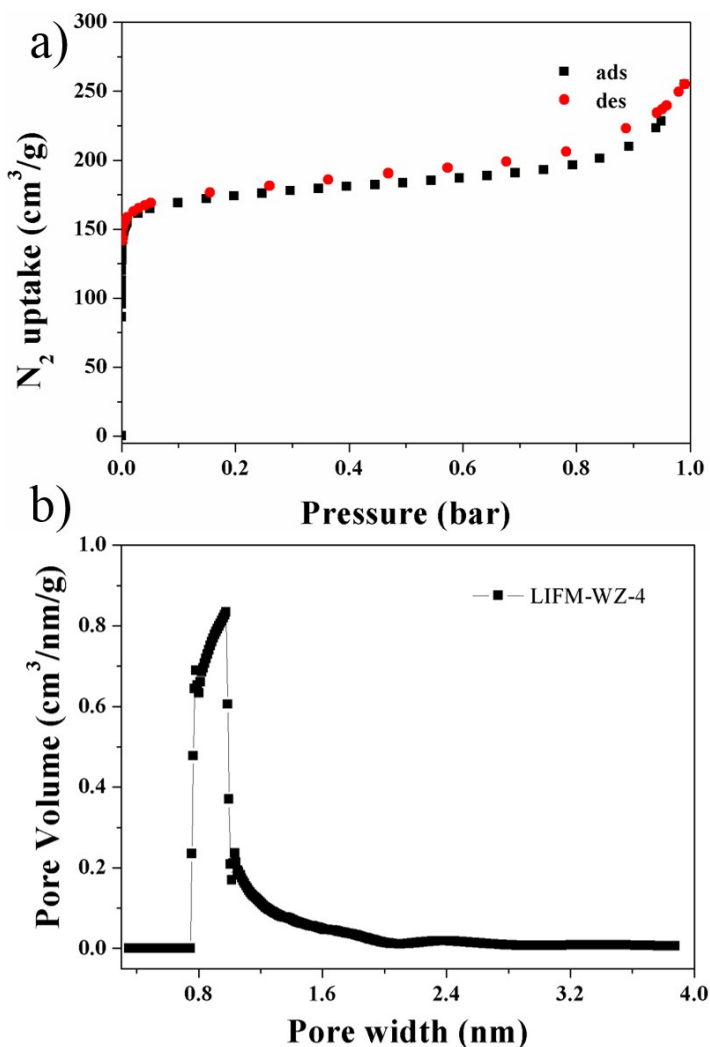


Figure S5. a) The N_2 sorption isotherm of LIFM-WZ-4 at 77 K, and b) pore size distribution analyzed with SF method.

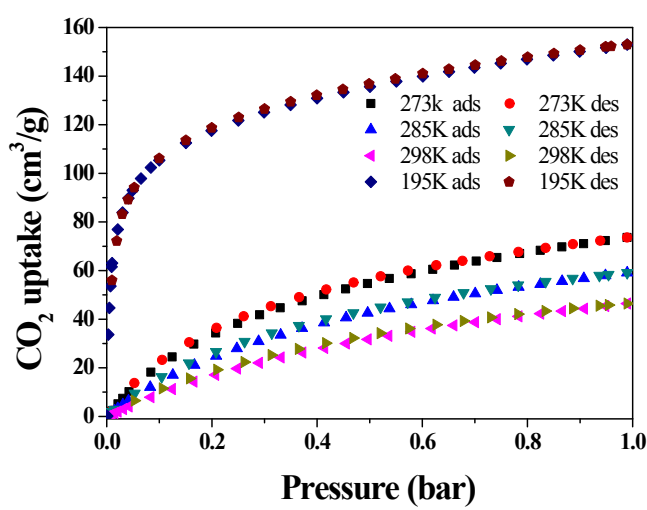


Figure S6. CO_2 sorption isotherms at different temperatures.

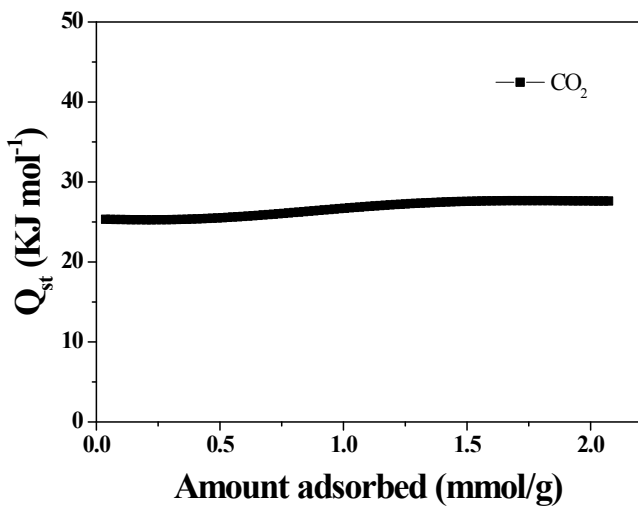


Figure S7. CO_2 isosteric heat.

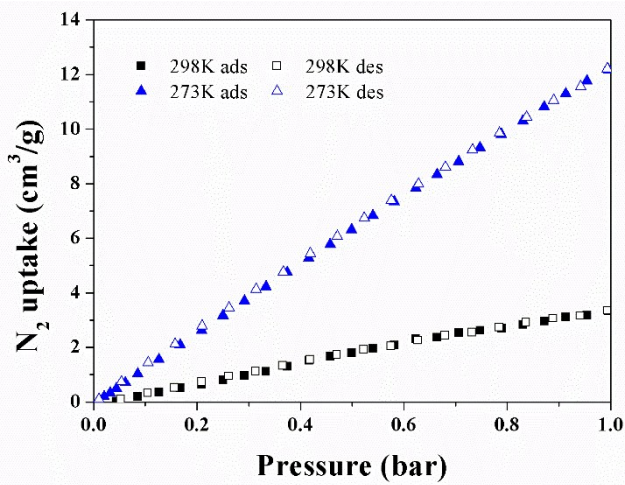


Figure S8. N_2 sorption isotherms of LIFM-WZ-4 at 298 and 273 K.

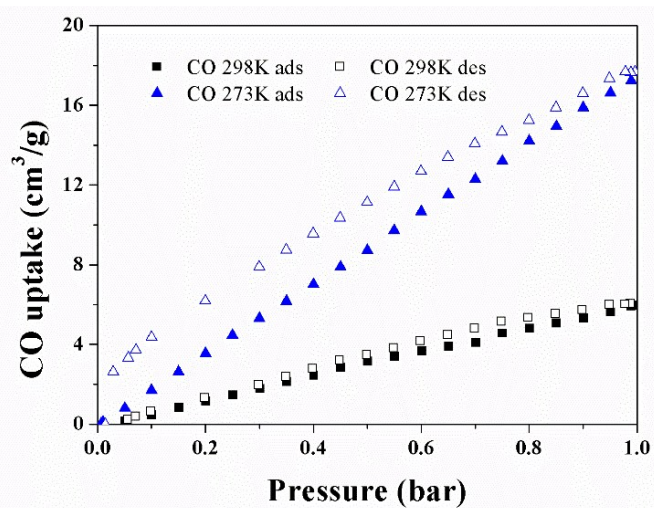


Figure S9. CO sorption isotherms of LIFM-WZ-4 at 298 and 273 K.

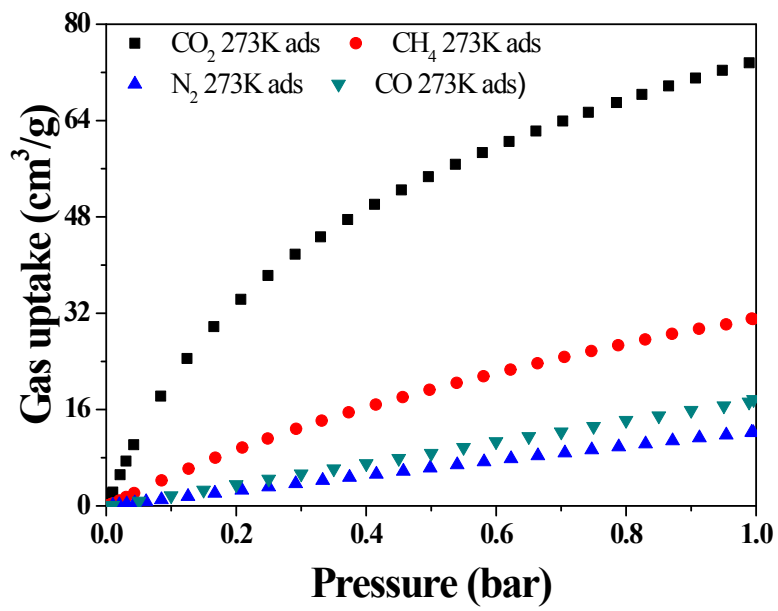


Figure S10. Selective uptake of CO_2 over CH_4 , N_2 and CO at 273 K.

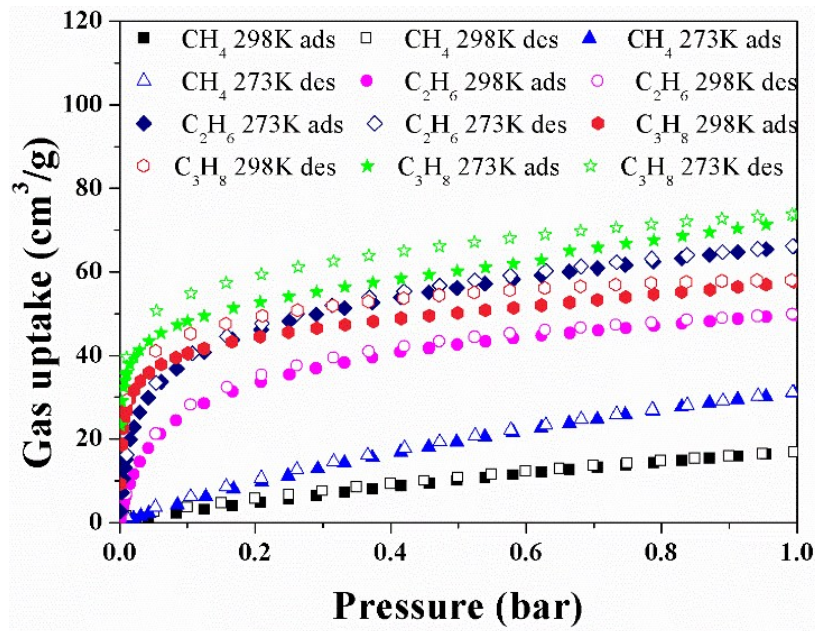


Figure S11. CH_4 , C_2H_6 and C_3H_8 sorption isotherms of LIFM-WZ-4 at 298 and 273 K.

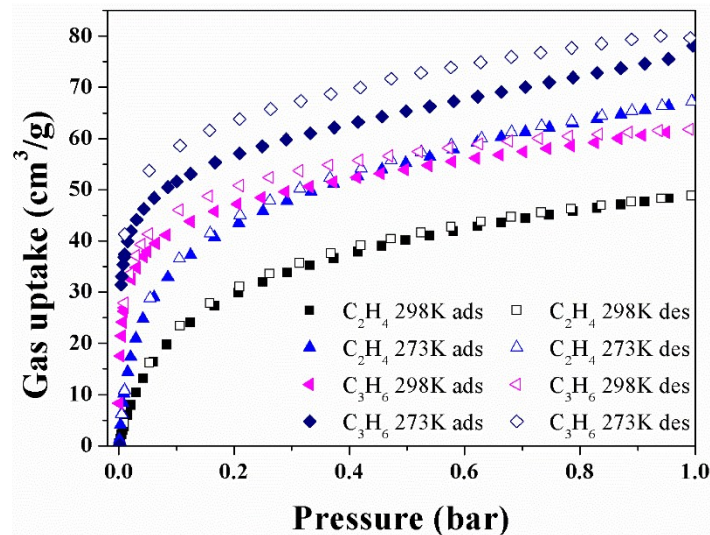


Figure S12. C_2H_4 and C_3H_6 sorption isotherms of LIFM-WZ-4 at 298 and 273 K.

4. Calculation of adsorption isosteric heats

The isosteric heats of CO_2 , CH_4 , C_2H_6 , C_3H_8 , C_2H_4 and C_3H_6 for LIFM-WZ-4 were calculated with adsorption data measured at 298 and 273K by the virial fitting method. A virial-type expression (eq. 1) which is composed of parameters a_i and b_i is used. In eq. 1, P is the pressure in torr, N is the adsorbed amount in $\text{mmol}\cdot\text{g}^{-1}$, T is the temperature in Kelvin, a_i and b_i are the virial coefficients which are independent of temperature, and m and n are the numbers of coefficients required to adequately describe the isotherms. The values of the virial coefficients a_0 through a_m were then applied to calculate the isosteric heat of adsorption (eq 2). In eq. 2, Q_{st} is the coverage-dependent isosteric heat of adsorption and R is the universal gas constant.

$$\ln P = \ln N + \frac{1}{T} \sum_{i=0}^m a_i N^i + \sum_{i=0}^n b_i N^i \quad \text{eq. 1}$$

$$Q_{st} = -R \sum_{i=0}^m a_i N^i \quad \text{eq. 2}$$

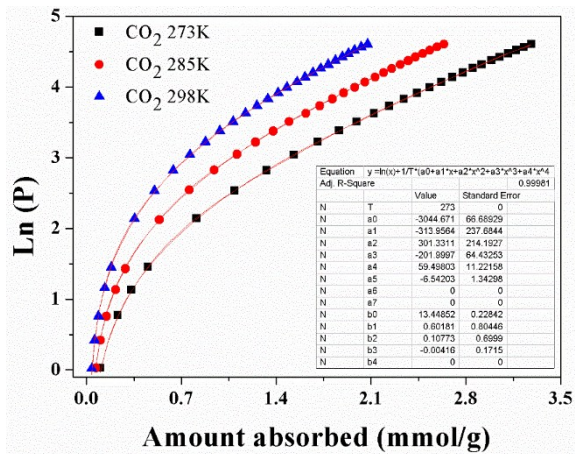


Figure S13. Virial fitting (lines) of the CO_2 adsorption isotherms (points) of LIFM-WZ-4 measured at 273, 285 and 298 K.

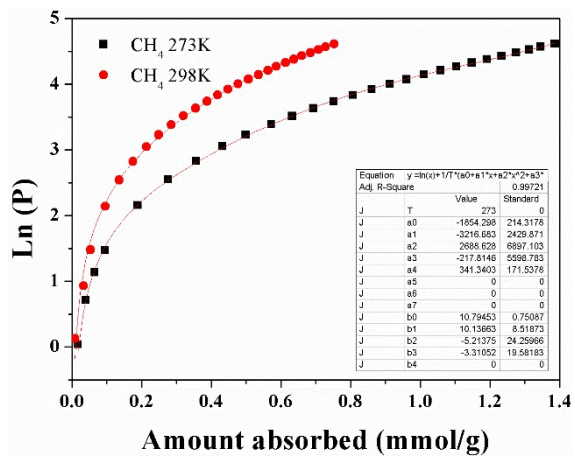


Figure S14. Virial fitting (lines) of the CH_4 adsorption isotherms (points) of LIFM-WZ-4 measured at 273 and 298 K.

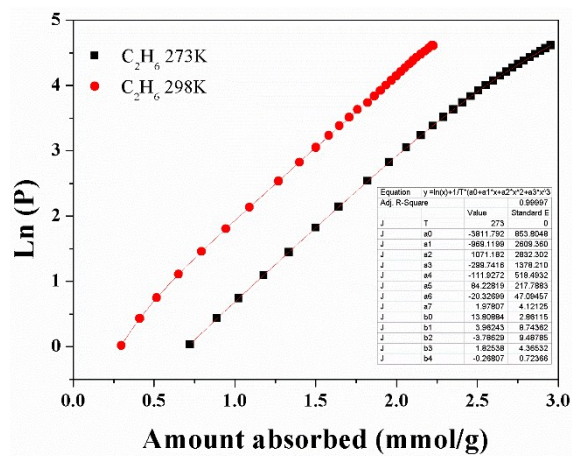


Figure S15. Virial fitting (lines) of the C_2H_6 adsorption isotherms (points) of LIFM-WZ-4 measured at 273 and 298 K.

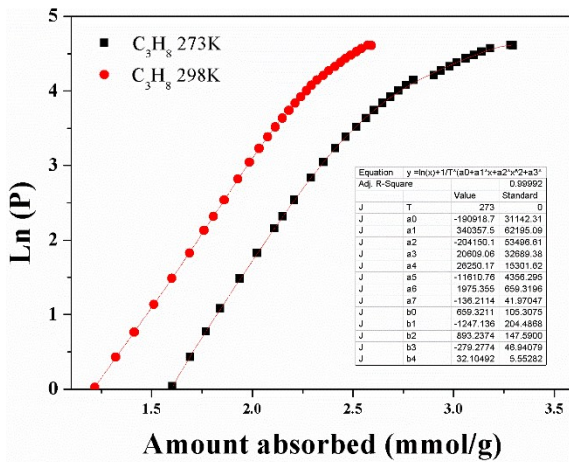


Figure S16. Virial fitting (lines) of the C_3H_8 adsorption isotherms (points) of LIFM-WZ-4 measured at 273 and 298 K.

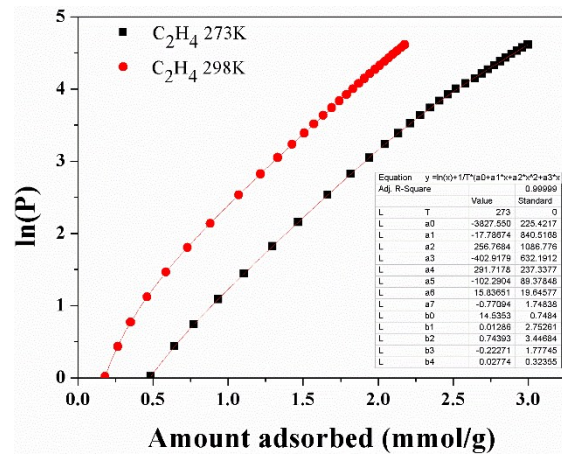


Figure S17. Virial fitting (lines) of the C_2H_4 adsorption isotherms (points) of LIFM-WZ-4 measured at 273 and 298 K.

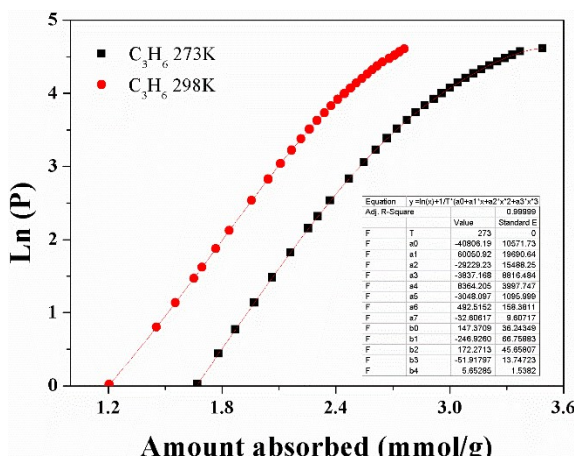


Figure S18. Virial fitting (lines) of the C_3H_6 adsorption isotherms (points) of LIFM-WZ-4 measured at 273 and 298 K.

5. IAST Selectivity

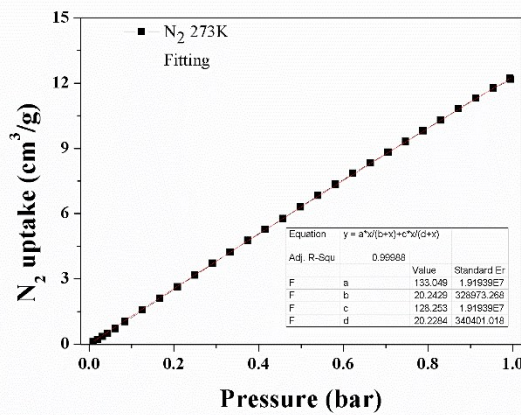
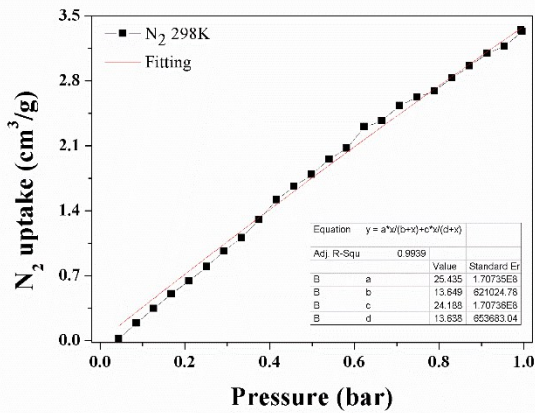
The experimental isotherm data for pure CO₂, C_xH_y (measured at 273 K and 298 K) were fitted using a Langmuir Freundlich (LF) model:

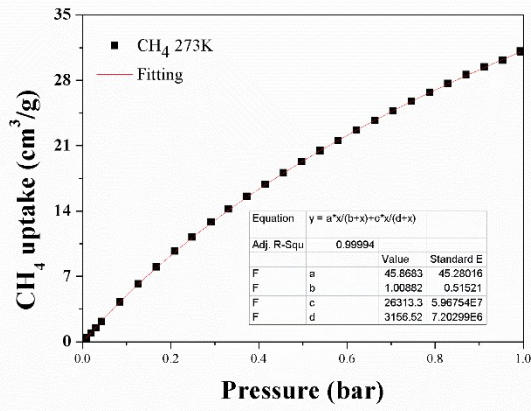
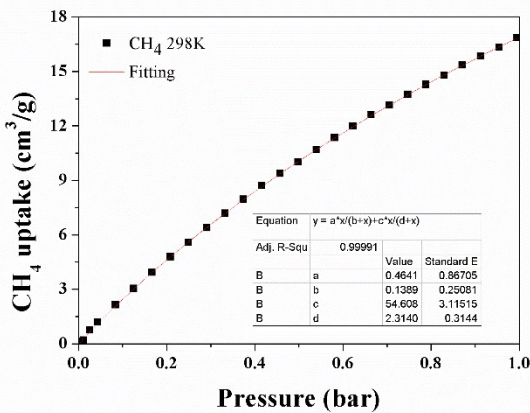
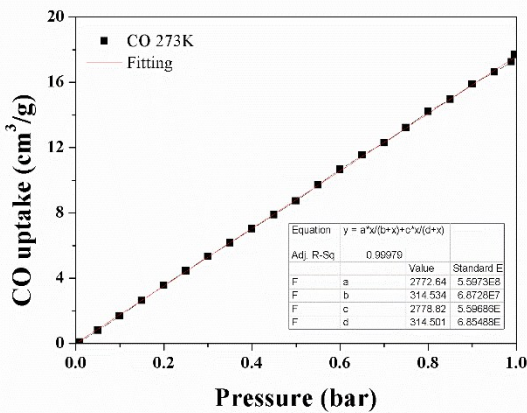
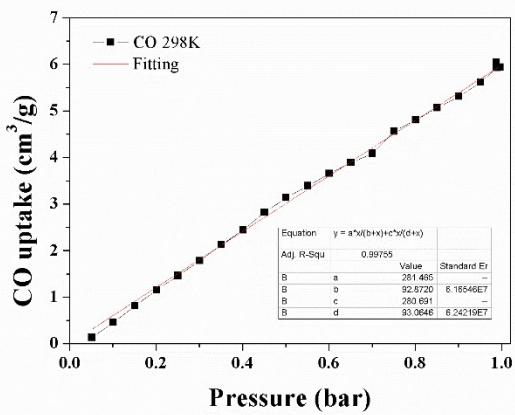
$$q = \frac{a * b * p^1 / n}{1 + b * p^1 / n}$$

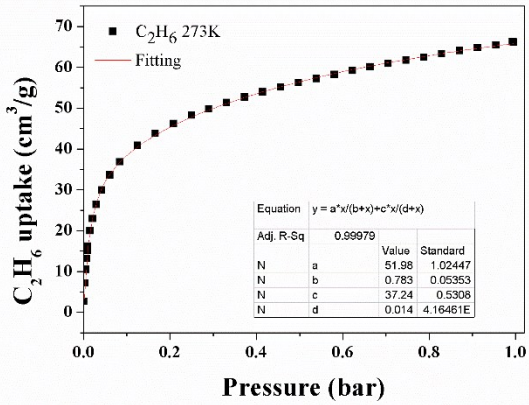
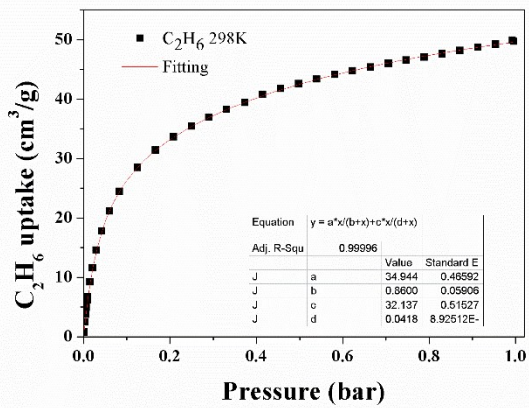
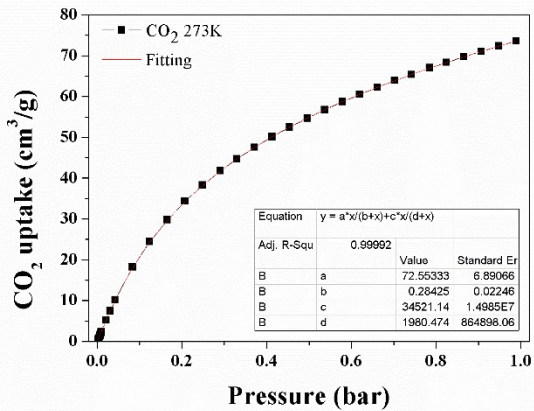
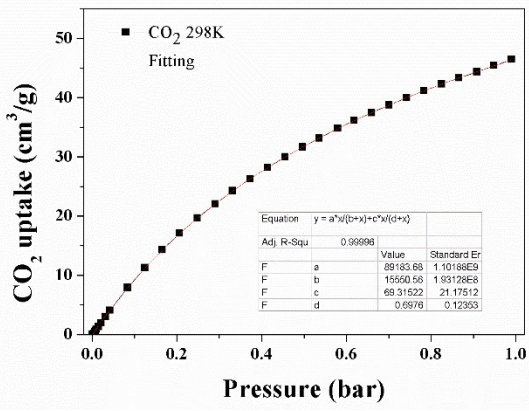
Where q and p is the adsorbed amount and pressure of component i , respectively. The adsorption selectivities for binary mixtures of CO₂/N₂, CO₂/CH₄, C_xH_y/CH₄ defined by

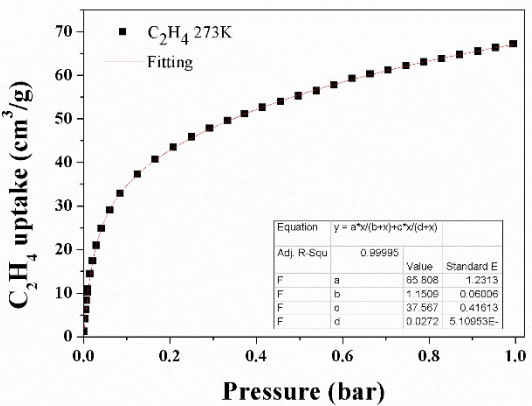
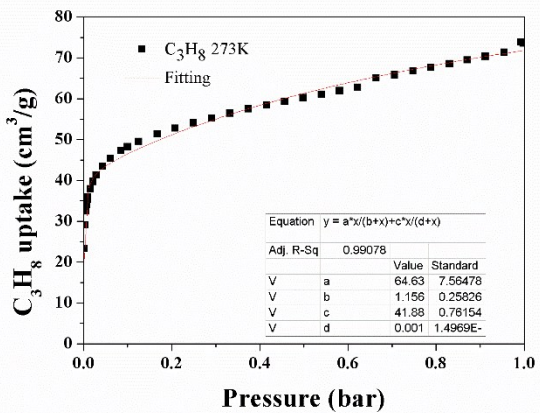
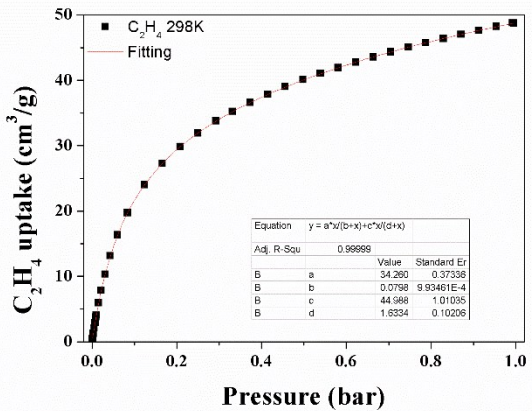
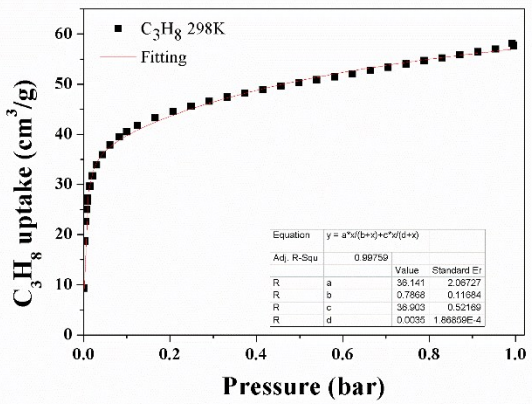
$$S_{i/j} = \frac{x_i}{x_j} * \frac{y_j}{y_i}$$

were calculated using the Ideal Adsorption Solution Theory (IAST) of Myers and Prausnitz. Where x_i is the mole fraction of component i in the adsorbed phase and y_i is the mole fraction of component i in the bulk.









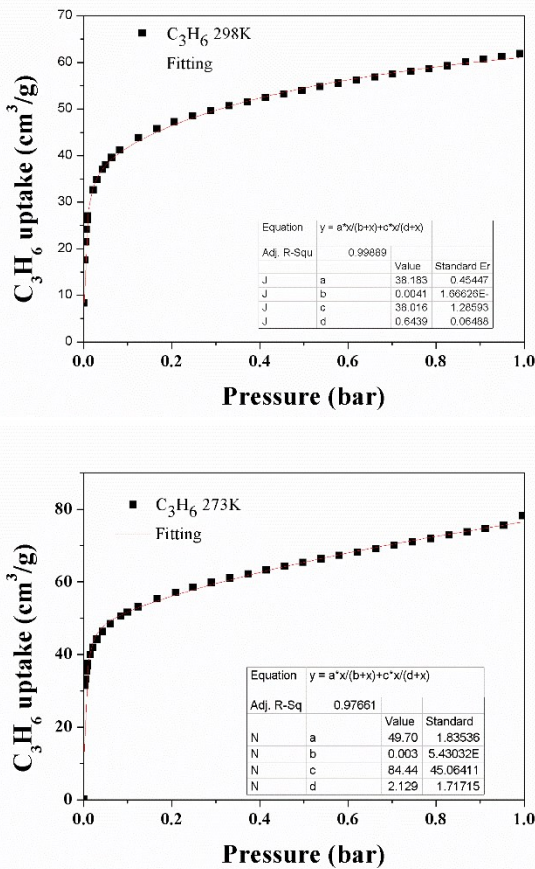


Figure S19. N₂, CO₂, CO, CH₄, C₂H₄, C₂H₆, C₃H₈ and C₃H₆ adsorption isotherms of LIFM-WZ-4 at 273 and 298 K fitted by LF model.

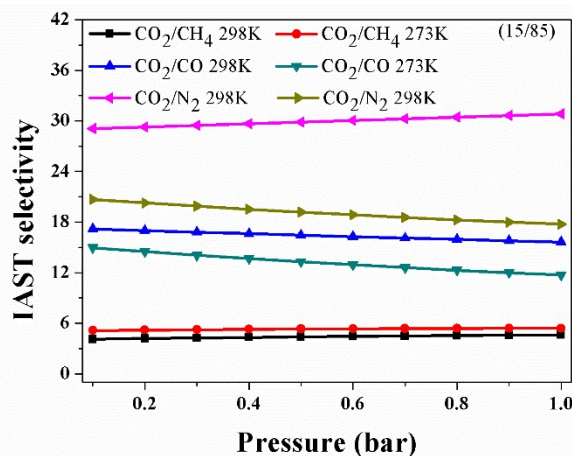
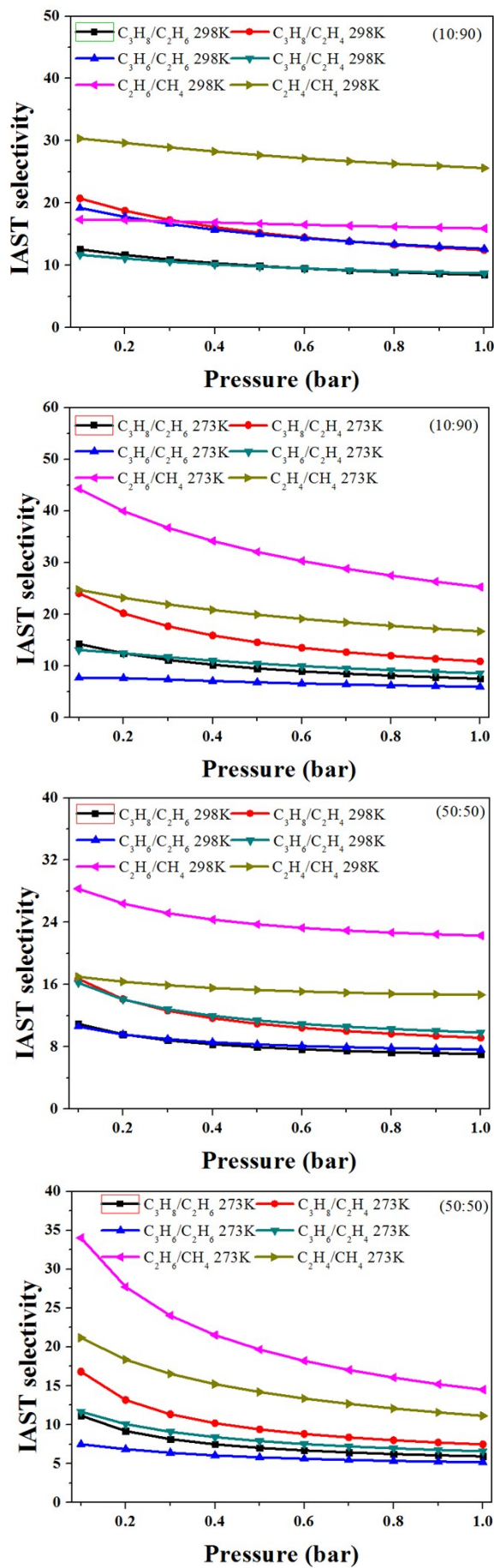


Figure S20. Selectivities of CO₂/CH₄, CO₂/CO and CO₂/N₂ (15:85) at 298 and 273 K calculated from IAST method.



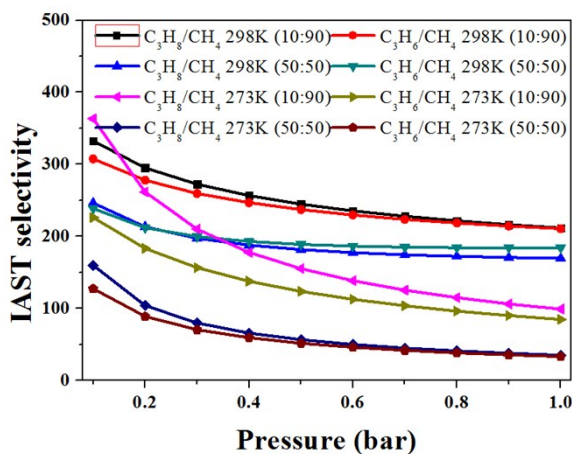


Figure S21. Selectivities of C₃/C₂, C₃/CH₄ and C₂/CH₄ (50:50/10:90) at 298 and 273 K calculated from IAST method.

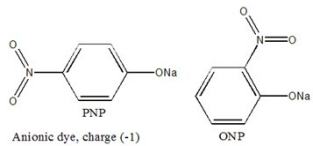
Table S4 IAST selectivities of various binary- gas mixtures (1 bar).

Mixtures	T(K)	IAST selectivity
		(10:90)/(50:50)
C ₃ H ₈ /C ₂ H ₆	298	8.5/7.1
	273	7. 6/5.9
C ₃ H ₈ /C ₂ H ₄	298	12.4/9.2
	273	10.9/7.5
C ₃ H ₈ /CH ₄	298	211.8/169.7
	273	99.0/35.2
C ₃ H ₆ /C ₂ H ₆	298	8.7/7. 7
	273	6.0/5.2
C ₃ H ₆ /C ₂ H ₄	298	12.7/9.9
	273	8.6/6.6
C ₃ H ₆ /CH ₄	298	210.8/184.3
	273	84.7/33.2
C ₂ H ₆ /CH ₄	298	25.6/22.3
	273	25.3/14.5
C ₂ H ₄ /CH ₄	298	15.9/14.7
	273	16.7/11.1

6. Organic dyes with different sizes and charges

Table S5. Organic dyes with different sizes and charges

Name	Neutral		Anionic		Cationic			
	DY	SD-I	AO ⁻	MO ⁻	MB ⁺	CV ⁺	BR ⁺	RB ⁺
Charge	0	0	-1	-1	+1	+1	+1	+1
x(Å)	4.02	3.68	5.46	5.31	4.00	4.00	4.99	6.79
y(Å)	6.76	9.74	9.76	7.25	7.93	12.97	9.40	11.80
z(Å)	14.21	13.55		15.62	17.39	16.34	13.74	15.68



DY: dimethyl yellow; SD-I: Sudan-I; AO⁻: Acid orange; MO⁻: methyl orange; MB⁺: methylene blue; CV⁺: crystal violet; BR⁺: basic red; RB⁺: rhodamine B; ONP⁻: ortho-nitrophenolate; PNP⁻: para-nitrophenolate.

7. Dye adsorption test results

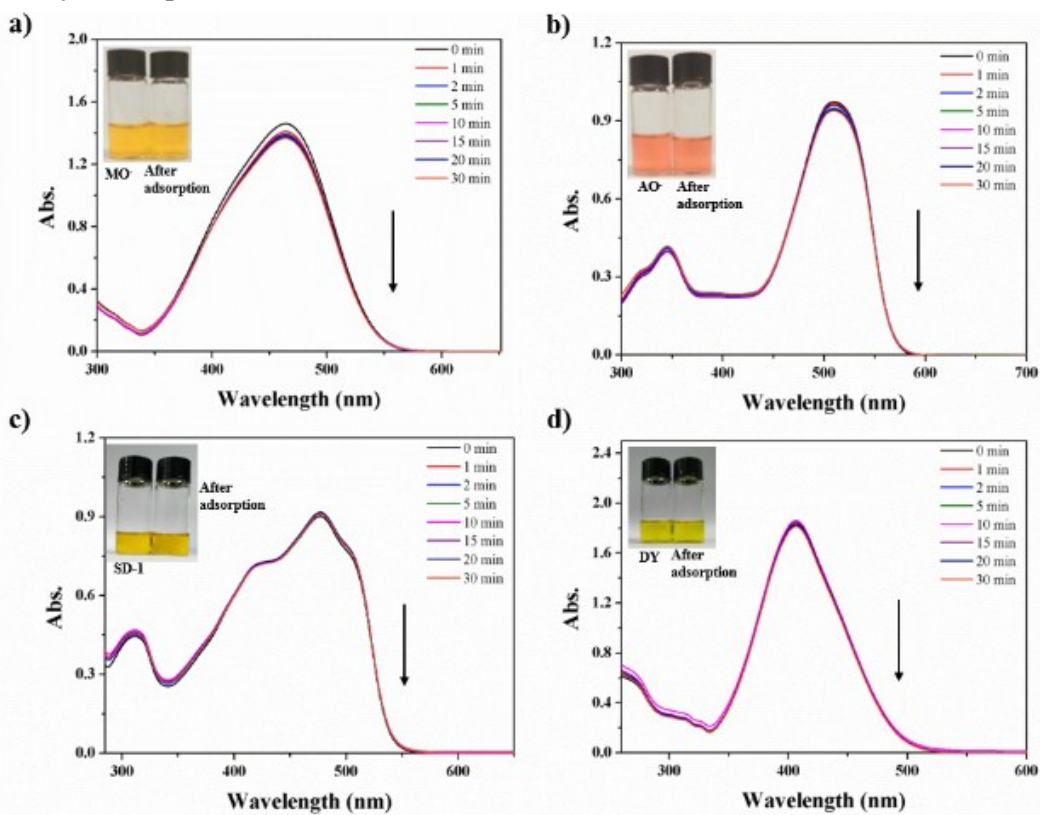


Figure S22. Temporal evolution of UV-Vis absorption spectra of 20 mL aqueous solution containing a) MO⁻, b) AO⁻, c) SD-1 and d) DY (20 mg L⁻¹) with LIFM-WZ-4 (2 mg) as adsorbent. Inserted graph shows the color of dye solution before and after adsorption.

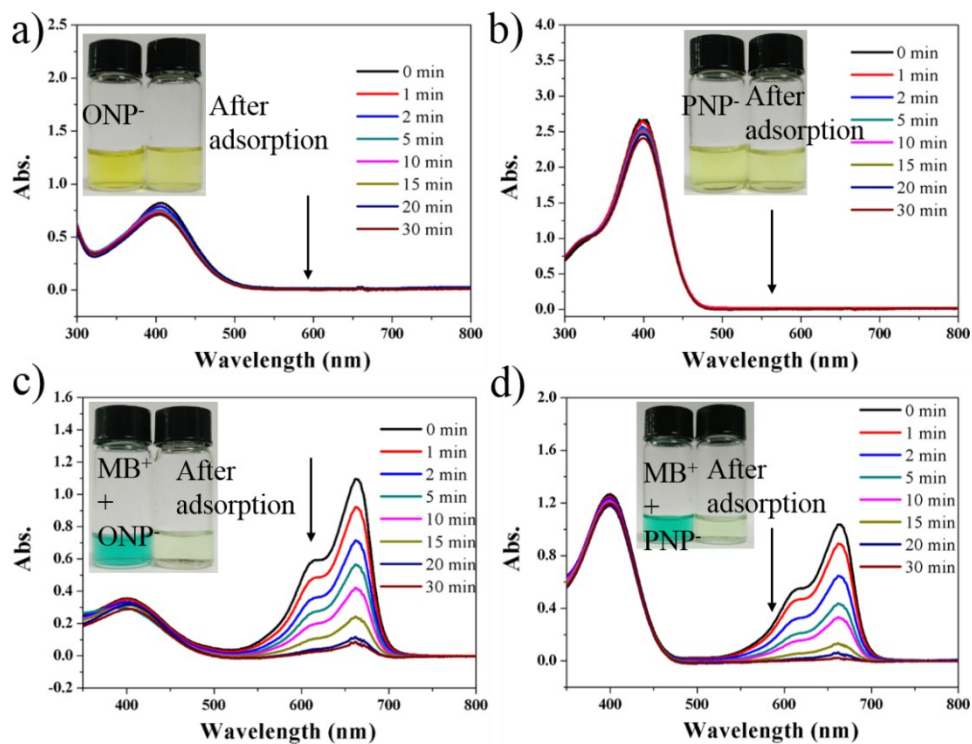


Figure S23. a, b) Temporal evolution of UV-Vis absorption spectra of 20 mL aqueous solution

containing ONP⁻ and PNP⁻ (40 mg L^{-1} for ONP⁻ and PNP⁻) with LIFM-WZ-4 (2 mg) as adsorbent, respectively. c, d) binary-component dyes adsorption with 2 mg LIFM-WZ-4 (40 mg L^{-1} aqueous solution for ONP⁻ and PNP⁻ and 20 mg L^{-1} aqueous solution for MB⁺ with the volume ratio in binary-solution is 20 ml:20 ml). Inserted graph shows the color of dye solution before and after adsorption.

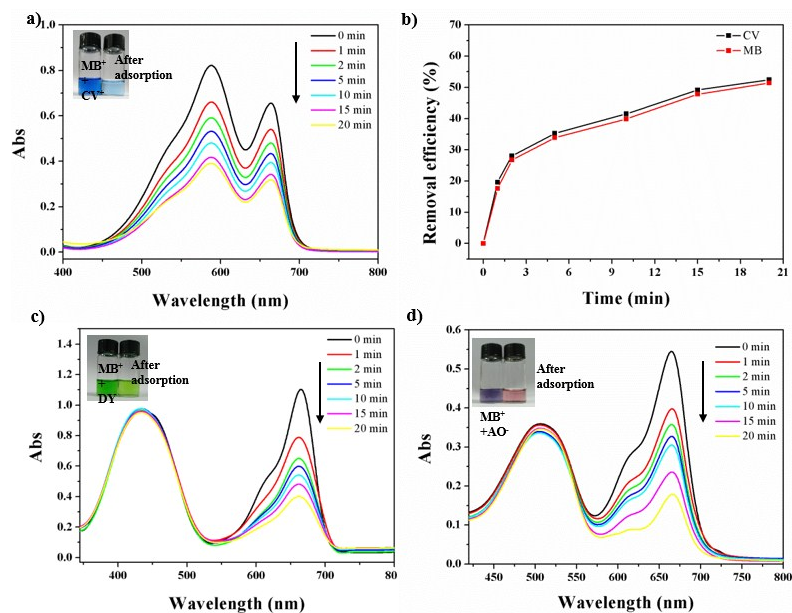


Figure S24. UV-Vis absorption spectra of binary-component dyes adsorption with 2 mg LIFM-WZ-4. a) MB⁺/CV⁺, c) MB⁺/DY, d) MB⁺/AO⁻, and b) removal efficiency of MB⁺/CV⁺. Inserted graphs reveal the color of two-component dyes solution before and after 20-min adsorption. Condition: 10 mg L^{-1} aqueous solution for each dye, and the binary-component volume ratio is 20 ml: 20 ml.

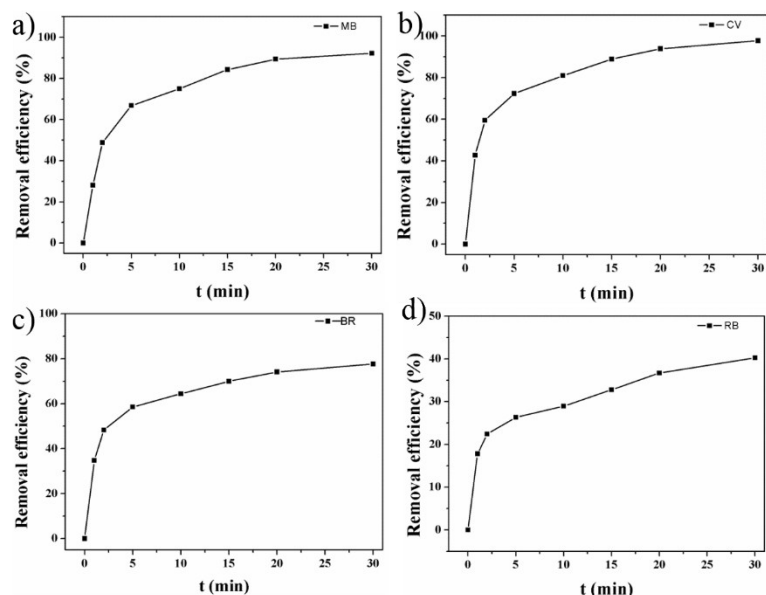


Figure S25. The removal efficiency of LIFM-WZ-4 with time for single dye, a) MB⁺, b) CV⁺, c) BR⁺, and d) RB⁺ (removal efficiency = $(c_0 - c_t)/c_0 \times 100\%$, c_0 represents the original concentration and c_t represents the instantaneous concentration at moment t).

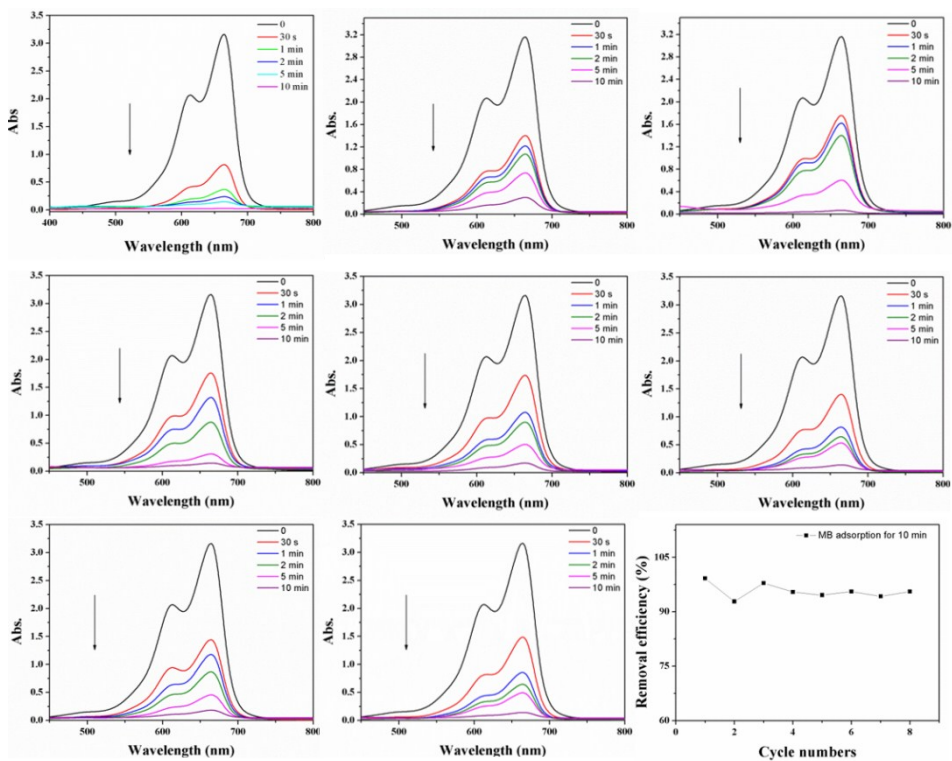


Figure S26. Eight runs of recycling adsorption experiments of MB^+ by LIFM-WZ-4 (5 mg powders in 20 ml aqueous solution with the MB^+ concentration of $20 \text{ mg}\cdot\text{L}^{-1}$).

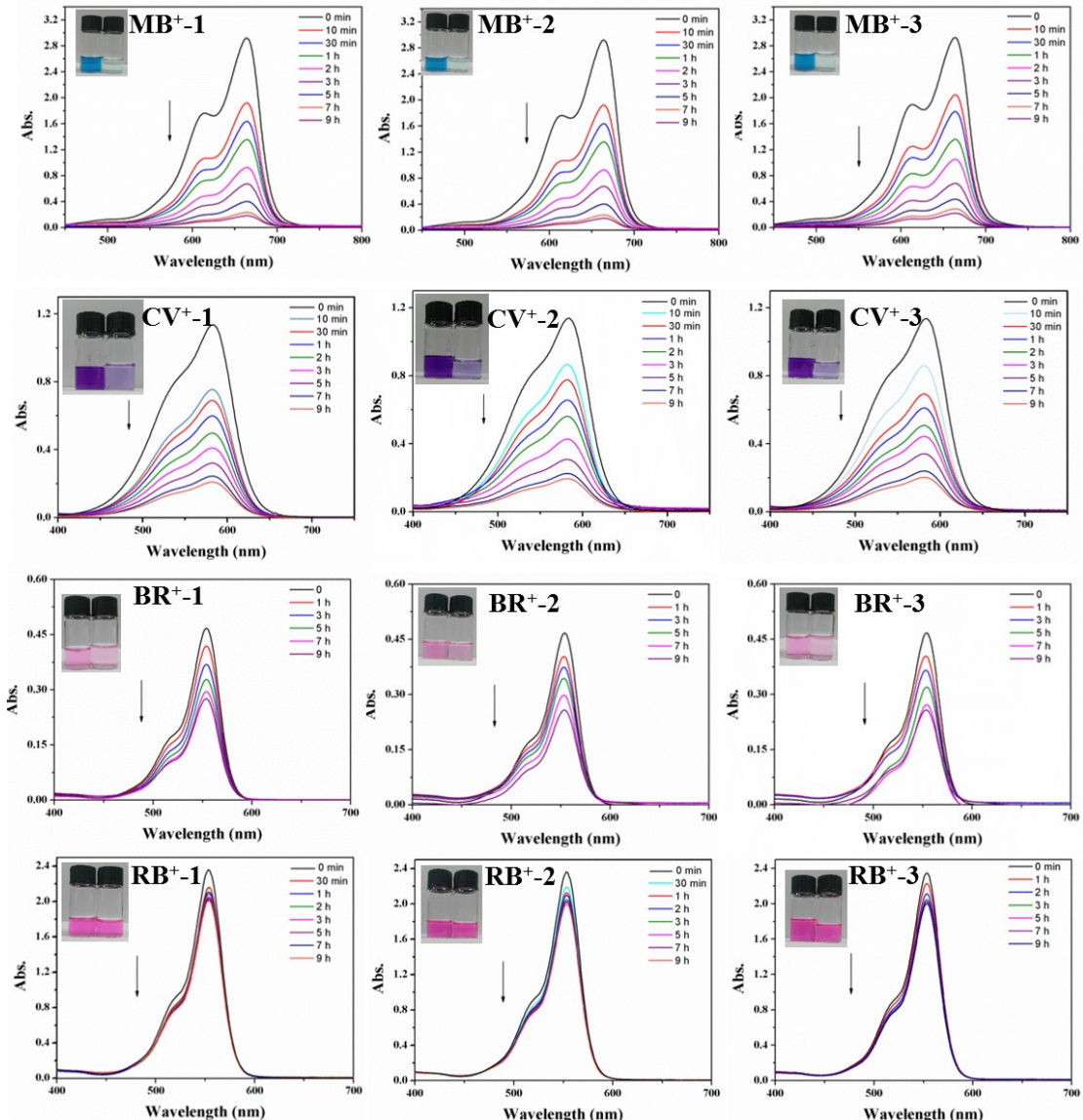


Figure S27. Temporal evolution of UV-Vis absorption spectra of MB^+ , CV^+ , BR^+ , and RB^+ in 80 ml aqueous solution (MB^+ , CV^+ and BR^+ for 20 mg/L, RB^+ for 10 mg/L) containing 1 mg LIFM-WZ-4, respectively. The photographs show the colors of solution before and after 9 h of organic dye absorption.

Table S6. The organic dye adsorption capacity of 1 mg LIFM-WZ-4 after 9 h (three parallel tests for each dye).

Dyes	Test 1	Test 2	Test 3	Average
MB^+	1500.4	1496.8	1478.8	1492.0
CV^+	653.2	670.1	657.8	660.4
BR^+	394.5	358.6	328.7	360.6
RB^+	61.0	62.9	61.6	61.8

Table S7. Adsorption capacity of MB⁺ by various types of adsorbents.

No.	Type	Adsorbent	Adsorption capacity (mg g ⁻¹)	Ref.
1	Hybrid material	Fe ₃ O ₄ @MnO ₂ core–shell nanocomposite	9.71	1
2	Hybrid material	MMWCNT	11.86	2
3	Hybrid material	Oak sawdust	29.94	3
4	Hybrid material	GO/Fe ₃ O ₄ nanohybrids	32	4
5	Hybrid material	GO	43.5	5
6	Hybrid material	MgO nanoparticles	93	6
7	Hybrid material	MCGO	95.16	5
8	Hybrid material	HKUST-1/GO	183.5	7
9	Hybrid material	pPDA-GOH	235.8	8
10	Hybrid material	Go-based hydrogels	334.45	9
11	Hybrid material	GO sponge	396.83	10
12	Hybrid material	MgSi/RGO	433	11
13	Hybrid material	Co/NPC-800	500	12
14	Hybrid material	GO-DETA hydrogel	884.96	9
15	Polymer	PVA/PAA/GO-COOH@PDA composite membrane	26.92	13
16	Polymer	D@GO-COOH@(PEI/PAA)	43.86	13
17	Polymer	PVDF/PDA membranes	172.3	14
18	Polymer	PDA-graphene aerogel	300	15
19	Polymer	PVI-TFS	476	16
20	Polymer	LC-network	980	17
21	Polymer	PVA/PAA@PDA-15 membrane	1147	18
22	Polymer	PDA/PEI@PVA/PEI	1290	19
23	Neutral MOF	MOF-3	30	20

24	Neutral MOF	MOF-1	105	²⁰
25	Neutral MOF	MOF-235	252	²¹
26	Anionic MOF	Sr-BTTC	270	²²
27	Neutral MOF	MOF-2	318	²⁰
28	Anionic MOF	[Zn ₂ (btb) ₂ (bbis)](Me ₂ NH ₂) ₂	348	²³
29	Anionic MOF	[(CH ₃) ₂ NH ₂]Cd(MIPA)]	395.17	²⁴
30	Neutral MOF	MIL-100(Cr)	645	²⁵
31	Anionic MOF	In-MOF	724.6	²⁶
32	Neutral MOF	MIL-100(Fe)	736	²⁵
33	Anionic MOF	amino-MIL-101(Al)	762	²⁷
34	Neutral MOF	NH ₂ -MIL-125(Ti)	862	²⁸
35	Neutral MOF	ZJU-24-0.89	902	²⁹
36	Anionic MOF	LIFM-WZ-3	983	³⁰
37	Anionic MOF	FJI-C2	1323	³¹
38	Neutral MOFs	LIFM-WZ-4	1492.0	This work

8. Kinetic and thermodynamic feature research

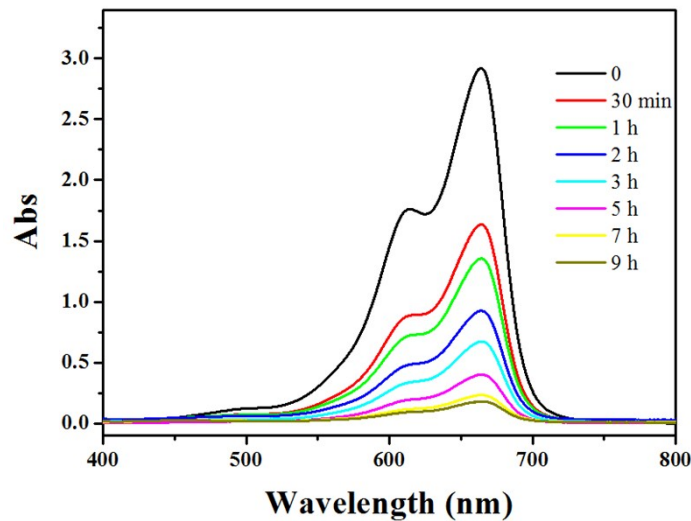


Figure S28. UV-Vis spectrum of kinetic experiment, and 1 mg of LIFM-WZ-4 immersed in 80 ml MB^+ aqueous solution (20 mg L^{-1}).

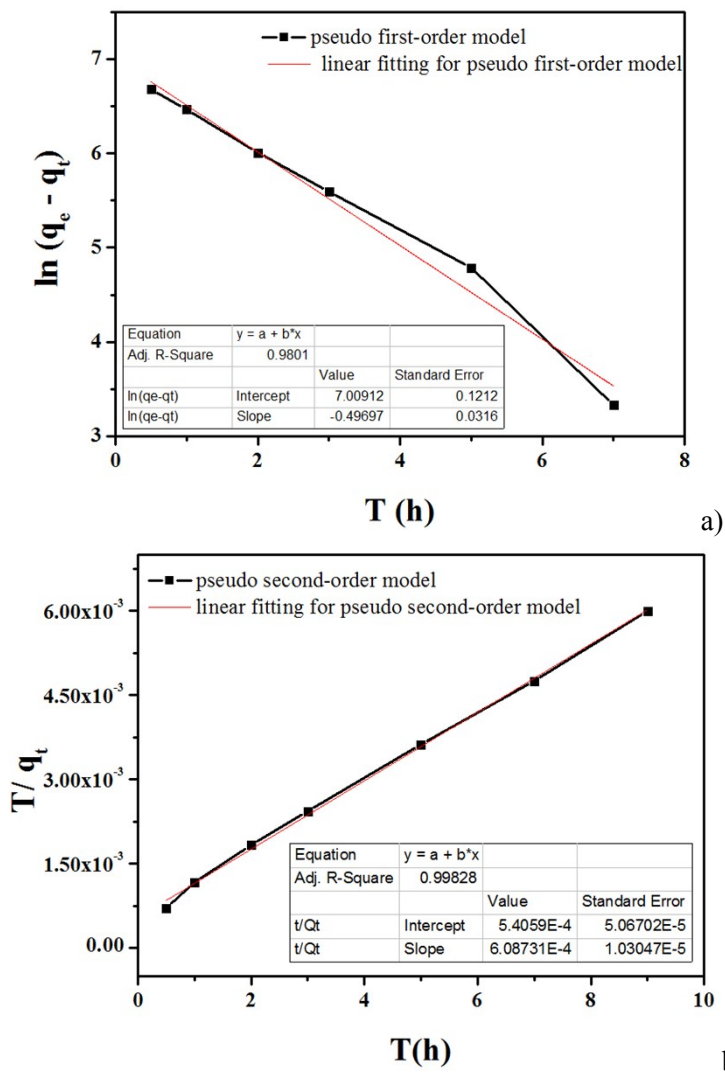


Figure S29. (a) Linear simulation of pseudo-first order reaction. (b) Linear simulation of

pseudo-second order reaction.

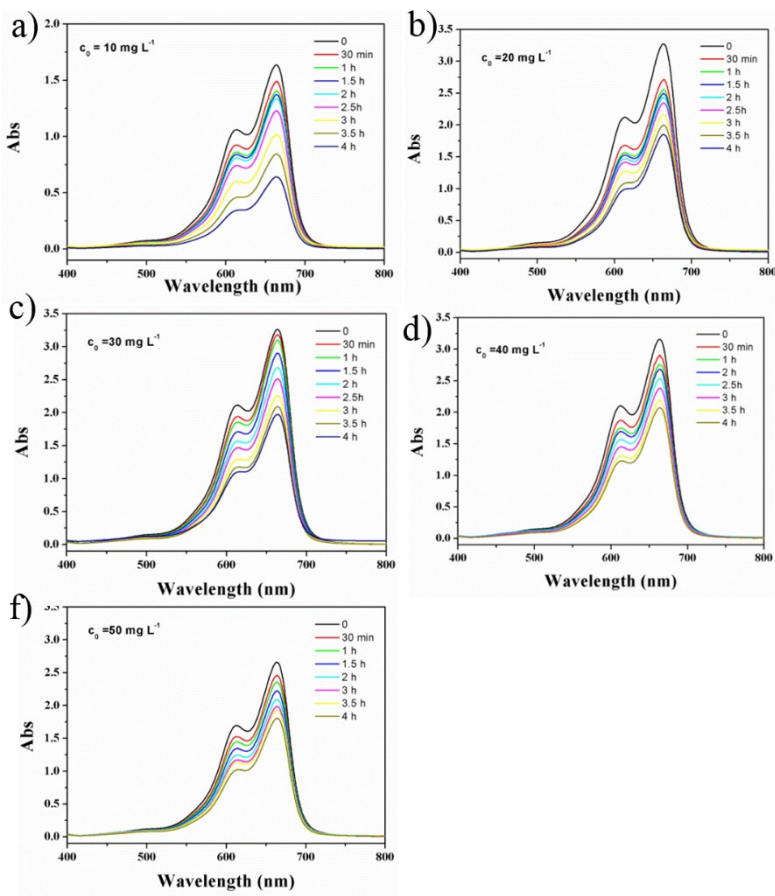
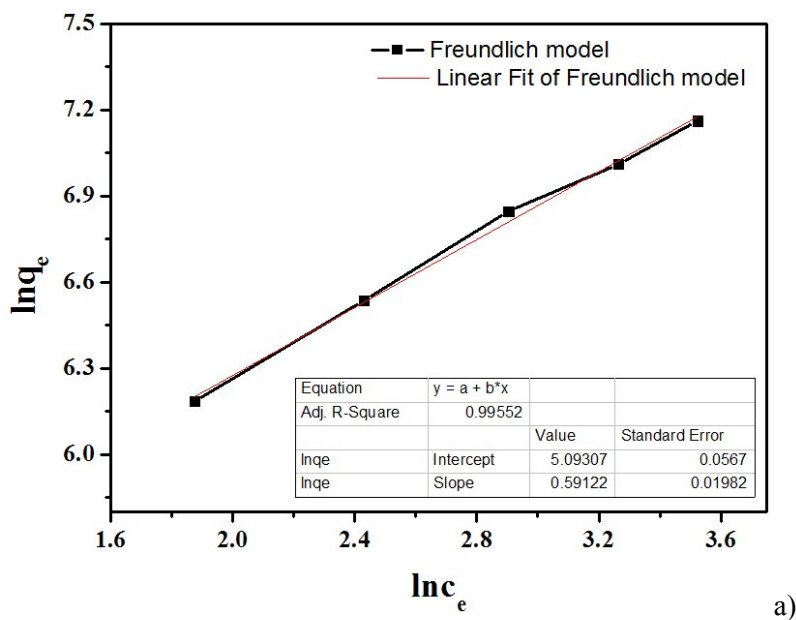


Figure S30. UV-Vis spectrum of isothermal model experiment. Initial concentrations of MB^+ solution are $10, 20, 30, 40, 50 \text{ mg L}^{-1}$ respectively.



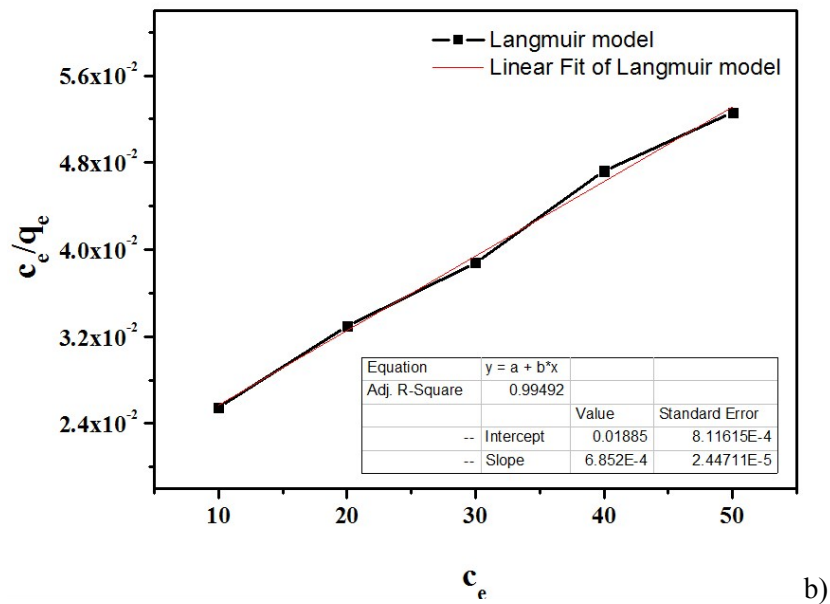


Figure S31. (a) Freundlich isothermal model of MB^+ adsorption by LIFM-WZ-4. (b) Langmuir isothermal model of MB^+ adsorption by LIFM-WZ-4.

Table S8. Fitted data for Langmuir isotherm model and Freundlich isotherm model

Isotherm model		LIFM-WZ-4
Langmuir	q_{max} (mg g ⁻¹)	1459.4279
	b (L·mg ⁻¹)	0.03640
	R ²	0.9949
Freundlich	k_f	162.8886
	n	1.6914
	R ²	0.9955

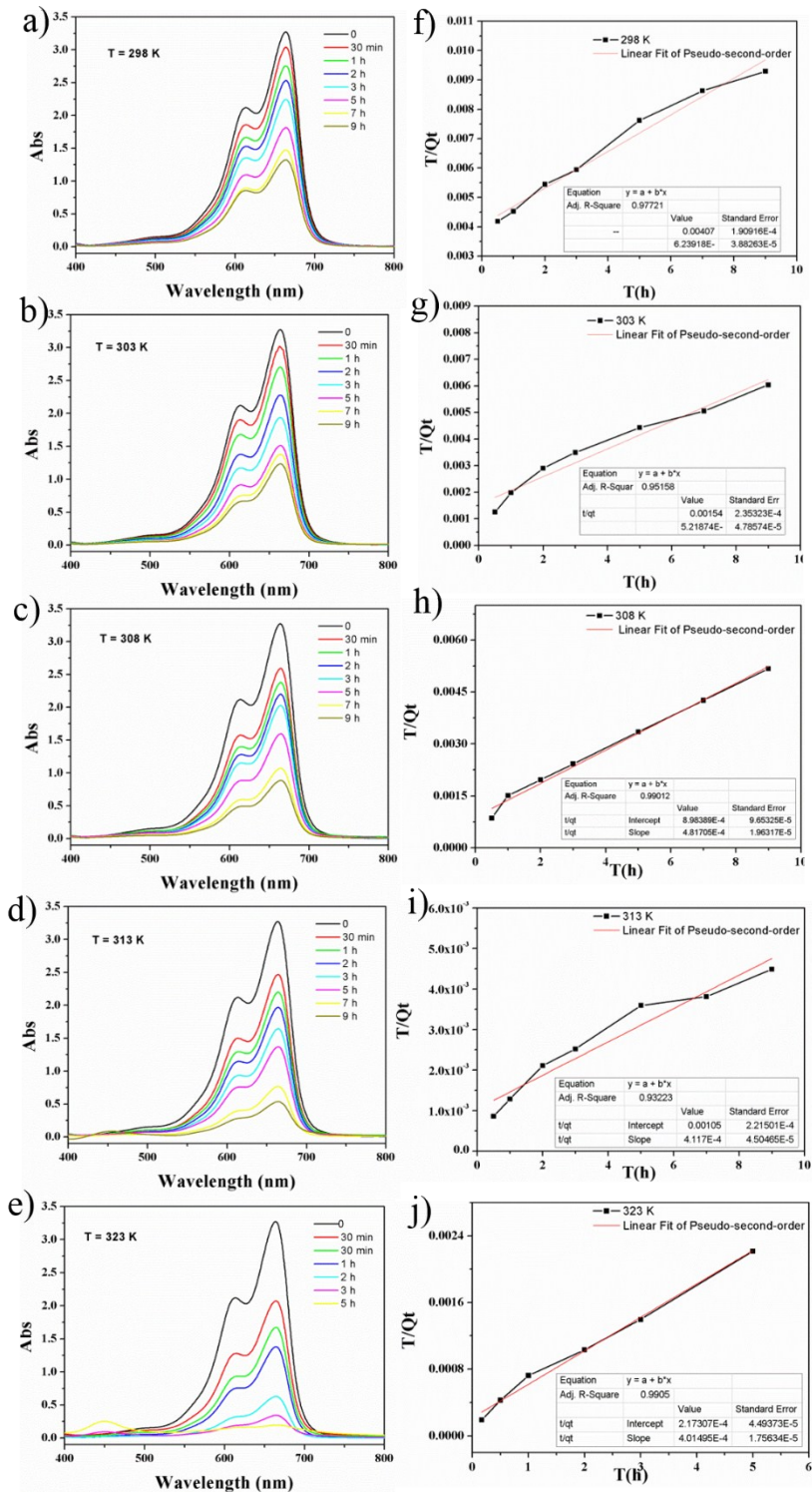


Figure S32. UV-Vis spectra of thermodynamic experiments. (a-e) Adsorption experiments were conducted under 298, 303, 308, 313 and 323 K, respectively. (f-j) Pseudo-second order fitting of MB^+ adsorption by LIFM-WZ-4 under different temperature.

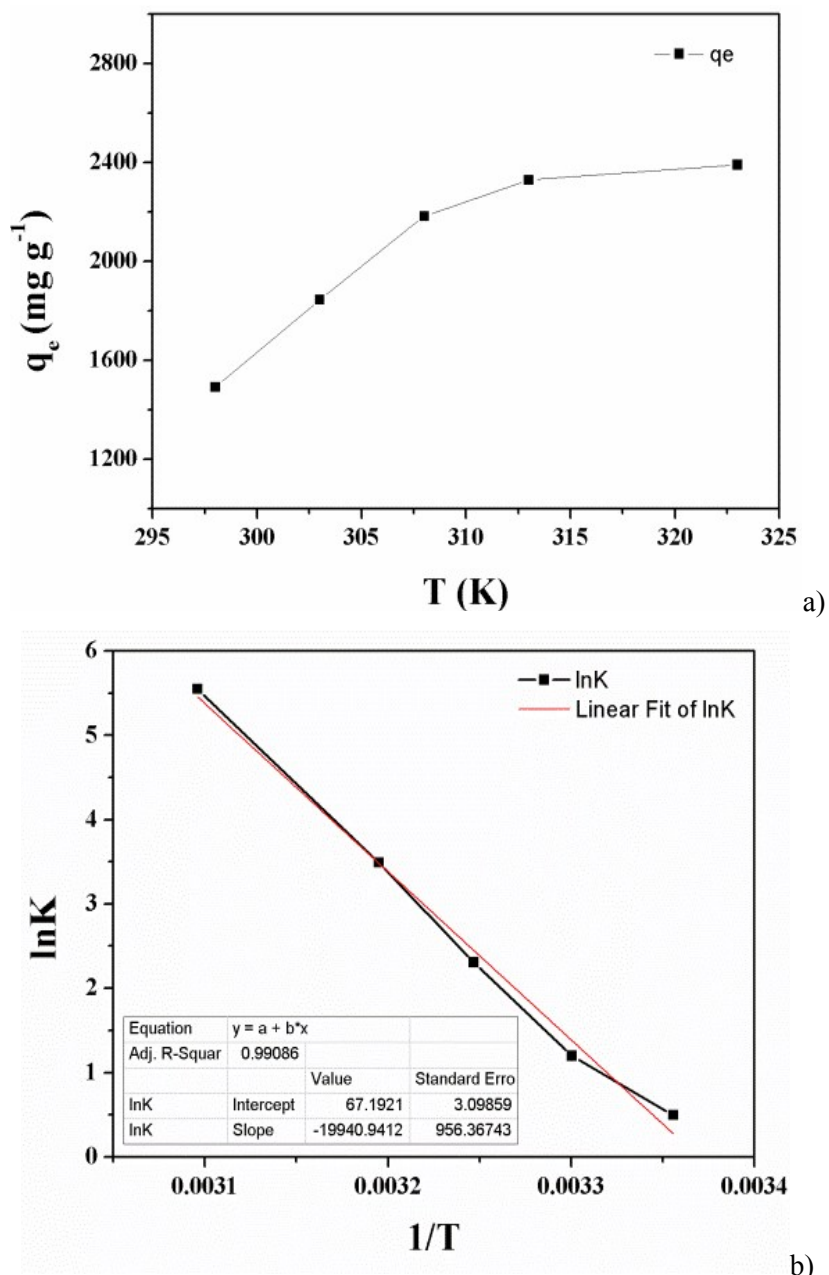


Figure S33. (a) Variation of adsorption amount of MB^+ with increasing temperature of the solution, and (b) the plot of $\ln K'_c$ versus $1/T$ to determine the thermodynamic parameters.

Table S9. Thermodynamic parameters calculated based on von't Hoff equation.

T (K)	ΔG^0 (kJ mol ⁻¹)	ΔH^0 (kJ mol ⁻¹)	ΔS^0 (J mol ⁻¹ K ⁻¹)	q_e	$\ln K'_c$
298	-1.7302			1602.7747	0.69835
303	-3.4673	136.1916	461.2491	1916.1860	1.37639
308	-5.2767			2128.8418	2.06063
313	-8.0082			2294.2778	3.07736

9. References

1. Wang, W.; Jiao, T.; Zhang, Q.; Luo, X.; Hu, J.; Chen, Y.; Peng, Q.; Yan, X.; Li, B., Hydrothermal synthesis of hierarchical core–shell manganese oxide nanocomposites as efficient dye adsorbents for wastewater treatment. *RSC Advances* **2015**, *5* (69), 56279-56285.
2. Gong, J.-L.; Wang, B.; Zeng, G.-M.; Yang, C.-P.; Niu, C.-G.; Niu, Q.-Y.; Zhou, W.-J.; Liang, Y., Removal of cationic dyes from aqueous solution using magnetic multi-wall carbon nanotube nanocomposite as adsorbent. *Journal of Hazardous Materials* **2009**, *164* (2), 1517-1522.
3. Ferrero, F., Dye removal by low cost adsorbents: Hazelnut shells in comparison with wood sawdust. *Journal of Hazardous Materials* **2007**, *142* (1), 144-152.
4. Jiao, T.; Liu, Y.; Wu, Y.; Zhang, Q.; Yan, X.; Gao, F.; Bauer, A. J. P.; Liu, J.; Zeng, T.; Li, B., Facile and Scalable Preparation of Graphene Oxide-Based Magnetic Hybrids for Fast and Highly Efficient Removal of Organic Dyes. *Scientific Reports* **2015**, *5*, 12451.
5. Fan, L.; Luo, C.; Li, X.; Lu, F.; Qiu, H.; Sun, M., Fabrication of novel magnetic chitosan grafted with graphene oxide to enhance adsorption properties for methyl blue. *Journal of Hazardous Materials* **2012**, *215-216*, 272-279.
6. Venkatesha, T. G.; Nayaka, Y. A.; Chethana, B. K., Adsorption of Ponceau S from aqueous solution by MgO nanoparticles. *Applied Surface Science* **2013**, *276*, 620-627.
7. Li, L.; Liu, X. L.; Geng, H. Y.; Hu, B.; Song, G. W.; Xu, Z. S., A MOF/graphite oxide hybrid (MOF: HKUST-1) material for the adsorption of methylene blue from aqueous solution. *Journal of Materials Chemistry A* **2013**, *1* (35), 10292-10299.
8. Luan, V. H.; Chung, J. S.; Kim, E. J.; Hur, S. H., The molecular level control of three-dimensional graphene oxide hydrogel structure by using various diamines. *Chemical Engineering Journal* **2014**, *246*, 64-70.
9. Zhu, K.; Jiao, T.; Zhang, L.; Xing, R.; Guo, R.; Zhou, J.; Hou, C.; Zhang, Q.; Peng, Q.; Li, X., Preparation and Absorption Capacity Evaluation of Composite Hydrogels via Graphene Oxide and Multi-Amine Molecules. *Science of Advanced Materials* **2016**, *8* (7), 1400-1407.
10. Liu, F.; Chung, S.; Oh, G.; Seo, T. S., Three-Dimensional Graphene Oxide Nanostructure for Fast and Efficient Water-Soluble Dye Removal. *ACS applied materials & interfaces* **2012**, *4* (2), 922-927.
11. Gui, C.-X.; Wang, Q.-Q.; Hao, S.-M.; Qu, J.; Huang, P.-P.; Cao, C.-Y.; Song, W.-G.; Yu, Z.-Z., Sandwichlike Magnesium Silicate/Reduced Graphene Oxide Nanocomposite for Enhanced Pb²⁺ and Methylene Blue Adsorption. *ACS applied materials & interfaces* **2014**, *6* (16), 14653-14659.
12. Torad, N. L.; Hu, M.; Ishihara, S.; Sukegawa, H.; Belik, A. A.; Imura, M.; Ariga, K.; Sakka, Y.; Yamauchi, Y., Direct Synthesis of MOF-Derived Nanoporous Carbon with Magnetic Co Nanoparticles toward Efficient Water Treatment. *Small* **2014**, *10* (10), 2096-2107.
13. Zhao, X.; Ma, K.; Jiao, T.; Xing, R.; Ma, X.; Hu, J.; Huang, H.; Zhang, L.; Yan, X., Fabrication of Hierarchical Layer-by-Layer Assembled Diamond-based Core-Shell Nanocomposites as Highly Efficient Dye Absorbents for Wastewater Treatment. *Scientific Reports* **2017**, *7*, 44076.
14. Ma, F.-f.; Zhang, N.; Wei, X.; Yang, J.-h.; Wang, Y.; Zhou, Z.-w., Blend-electrospun poly(vinylidene fluoride)/polydopamine membranes: self-polymerization of dopamine and the excellent adsorption/separation abilities. *Journal of Materials Chemistry A* **2017**, *5* (27), 14430-14443.
15. Cheng, C.; Li, S.; Zhao, J.; Li, X.; Liu, Z.; Ma, L.; Zhang, X.; Sun, S.; Zhao, C., Biomimetic assembly of polydopamine-layer on graphene: Mechanisms, versatile 2D and 3D architectures and pollutant disposal. *Chemical Engineering Journal* **2013**, *228*, 468-481.

16. Mi, H.; Jiang, Z.; Kong, J., Hydrophobic Poly(ionic liquid) for Highly Effective Separation of Methyl Blue and Chromium Ions from Water. *Polymers* **2013**, *5* (4).
17. van Kuringen, H. P. C.; Eikelboom, G. M.; Shishmanova, I. K.; Broer, D. J.; Schenning, A. P. H. J., Responsive Nanoporous Smectic Liquid Crystal Polymer Networks as Efficient and Selective Adsorbents. *Advanced Functional Materials* **2014**, *24* (32), 5045-5051.
18. Yan, J.; Huang, Y.; Miao, Y.-E.; Tjiu, W. W.; Liu, T., Polydopamine-coated electrospun poly(vinyl alcohol)/poly(acrylic acid) membranes as efficient dye adsorbent with good recyclability. *Journal of Hazardous Materials* **2015**, *283*, 730-739.
19. Zhu, Z.; Wu, P.; Liu, G.; He, X.; Qi, B.; Zeng, G.; Wang, W.; Sun, Y.; Cui, F., Ultrahigh adsorption capacity of anionic dyes with sharp selectivity through the cationic charged hybrid nanofibrous membranes. *Chemical Engineering Journal* **2017**, *313*, 957-966.
20. Yi, F. Y.; Li, J. P.; Wu, D.; Sun, Z. M., A Series of Multifunctional Metal-Organic Frameworks Showing Excellent Luminescent Sensing, Sensitization, and Adsorbent Abilities. *Chemistry* **2015**, *21* (32), 11475-82.
21. Haque, E.; Jun, J. W.; Jhung, S. H., Adsorptive removal of methyl orange and methylene blue from aqueous solution with a metal-organic framework material, iron terephthalate (MOF-235). *Journal of hazardous materials* **2011**, *185* (1), 507-11.
22. Shen, Y.; Fan, C.-C.; Wei, Y.-Z.; Du, J.; Zhu, H.-B.; Zhao, Y., An anionic zeolite-like metal-organic framework (AZMOF) with a Moravia network for organic dye absorption through cation-exchange. *Dalton transactions* **2016**, *45* (27), 10909-10915.
23. Guo, M.; Liu, S.; Guo, H.; Sun, Y.; Guo, X.; Deng, R., The mixed-ligand strategy to assemble a microporous anionic metal-organic framework: Ln(3+) post-functionalization, sensors and selective adsorption of dyes. *Dalton transactions* **2017**, *46* (43), 14988-14994.
24. Dong, B.-X.; Tang, M.; Liu, W.-L.; Wu, Y.-C.; Pan, Y.-M.; Bu, F.-Y.; Teng, Y.-L., Solvent- and Temperature-Induced Multiple Crystal Phases: Crystal Structure, Selective Adsorption, and Separation of Organic Dye in Three S-Containing {[Cd(MIPA)]n}n- Homologues. *Crystal Growth & Design* **2016**, *16* (11), 6363-6370.
25. Tong, M.; Liu, D.; Yang, Q.; Devautour-Vinot, S.; Maurin, G.; Zhong, C., Influence of framework metal ions on the dye capture behavior of MIL-100 (Fe, Cr) MOF type solids. *Journal of Materials Chemistry A* **2013**, *1* (30), 8534.
26. Li, Q.; Xue, D.-X.; Zhang, Y.-F.; Zhang, Z.-H.; Gao, Z.; Bai, J., A dual-functional indium-organic framework towards organic pollutant decontamination via physically selective adsorption and chemical photodegradation. *Journal of Materials Chemistry A* **2017**, *5* (27), 14182-14189.
27. Haque, E.; Lo, V.; Minett, A. I.; Harris, A. T.; Church, T. L., Dichotomous adsorption behaviour of dyes on an amino-functionalised metal-organic framework, amino-MIL-101(Al). *Journal of Materials Chemistry A* **2014**, *2* (1), 193-203.
28. Oveisi, M.; Asli, M. A.; Mahmoodi, N. M., MIL-Ti metal-organic frameworks (MOFs) nanomaterials as superior adsorbents: Synthesis and ultrasound-aided dye adsorption from multicomponent wastewater systems. *J Hazard Mater* **2018**, *347*, 123-140.
29. Zhang, Q.; Yu, J.; Cai, J.; Song, R.; Cui, Y.; Yang, Y.; Chen, B.; Qian, G., A porous metal-organic framework with -COOH groups for highly efficient pollutant removal. *Chemical communications* **2014**, *50* (92), 14455-14458.
30. Wang, Z.; Zhang, J.-H.; Jiang, J.-J.; Wang, H.-P.; Wei, Z.-W.; Zhu, X.; Pan, M.; Su, C.-Y., A stable metal cluster-metalloporphyrin MOF with high capacity for cationic dye removal. *Journal of Materials*

Chemistry A **2018**, *6* (36), 17698-17705.

31. Wang, X.-S.; Liang, J.; Li, L.; Lin, Z.-J.; Bag, P. P.; Gao, S.-Y.; Huang, Y.-B.; Cao, R., An Anion Metal-Organic Framework with Lewis Basic Sites-Rich toward Charge-Exclusive Cationic Dyes Separation and Size-Selective Catalytic Reaction. *Inorganic chemistry* **2016**, *55* (5), 2641-2649.